

NEOCIVET: Extraction of Cortical Surface and Analysis of Neonatal Gyrfication Using a Modified CIVET Pipeline

Hosung Kim¹, Claude Lepage², Alan C. Evans², A. James Barkovich¹, Duan Xu¹

¹ Department of Radiology and Biomedical Imaging, University of California, San Francisco, San Francisco, CA

² McConnell Brain Imaging Center, Montreal Neurological Institute and Hospital, McGill University, Montreal, Quebec, Canada
hosung.kim@ucsf.edu

Abstract. Cerebral cortical gyration becomes dramatically more complex in the fetal brain during the 3rd trimester of gestation; the process proceeds in a similar fashion *ex utero* in children who are born prematurely. To quantify this morphological development, it is necessary to extract the interface between gray matter and white matter. We employed the well-established CIVET pipeline to extract this cortical surface, with point correspondence across subjects, using a surface-based spherical registration. We developed a variant of the pipeline, called NEOCIVET, that addresses the well-known problems of poor and temporally-varying gray/white contrast in neonatal MRI. NEOCIVET includes a tissue classification strategy that combines i) local and global contrast features, ii) neonatal template construction based on age-specific subgroups, and iii) masking of non-interesting structures using label-fusion approaches. These techniques replaced modules that might be suboptimal for regional analysis of poor-contrast neonatal cortex. In the analysis of 43 preterm neonates, many with multiple scans (n=65; 28-40 wks PMA at scan), NEOCIVET identified increases in cortical folding over time in numerous cortical regions (mean curvature: +0.004/wk) while folding did not change in major sulci that are known to develop early (corrected $p < 0.05$). Cortical folding increase was disrupted in the presence of severe types of perinatal WM injury. The proposed pipeline successfully mapped cortical structural development, supporting current models of cerebral morphogenesis.

Keywords: neonatal brain MRI, cortical folding, surface extraction, CIVET.

1 Introduction

Cerebral cortical gyration is one of the most striking morphological changes that occur in the fetal brain during the 3rd trimester of gestation; the process proceeds in a similar manner *ex utero* in children who are born prematurely. To quantify such early morphological development, it is necessary to extract cortical surface, especially the interface of the gray matter (GM) and white matter (WM). Only a few packages [1, 2] have been proposed to perform this task. To enable regional analysis, they co-register

an individual lobar atlas to each subject's cortical surface. However, this approach lacks point-wise correspondence across subjects and, consequently, spatial sensitivity.

Pure surface-based packages such as the MNI's CIVET pipeline or FreeSurfer extract triangulated cortical surface [3, 4] and define point correspondence using surface-based spherical registration [5]. However, these packages have not been optimized for fetal/neonatal analyses. Different degrees of myelination, neuronal proliferation, and cell migration among various cortical and subcortical regions, which are distinctive features of developing brain, are manifested as regionally- and temporally-varying GM/WM contrast in structural MRI. This spatiotemporally dynamic tissue contrast challenges tissue classification techniques used in most pipelines since they are usually based on a tissue contrast histogram constructed from the whole brain across time.

Techniques that combine a feature of local intensity variations into the original classification scheme have recently been proposed. Among them, a level-set-based approach developed by Li et al. [6] displayed excellent segmentation performance in images with locally distorted intensity distribution. To enable the analysis of cortical morphology in neonates, we developed a variant of the CIVET pipeline, called NEOCIVET. This pipeline includes a number of new modifications and parameter tunings. In particular, we optimized Li's method for the cortical GM segmentation by including additional features. Also, we constructed age-specific surface templates to improve the surface registration performance across subjects.

2 Methods

NEOCIVET includes a series of image processing steps to achieve the goal of extracting the interface between GM and WM. Briefly we describe the flow of the pipeline as in Fig 1: **A)** MRI images underwent intensity non-uniformity correction using N3 [7]; **B)** These images were linearly registered to the NIH neonatal template that was averaged across 0-2 month-old babies (<http://www.bic.mni.mcgill.ca/ServicesAtlases/NIHPD-obj2>); **C)** We segmented the cerebrum and cerebellum using a patch-based brain extraction algorithm (BEaST) [8]; **D)** These masked brains were re-registered to the template to improve the intracranial fitting; **E)** MRI intensities were re-corrected using N3 and normalized within the brain mask; **F)** the GM and WM were classified within the mask using a level-set-based deformable model that uses global and local contrasts as well as a cortical thickness constraint. The intensity of CSF voxels neighboring the cortex or residing within the sulci resembled that of normal neonatal WM due to the partial volume effect. Thus, we corrected their classification in a post-processing step using their geometric characteristics: i.e., the CSF partial volumes located exterior to the GM were masked. We eroded WM voxels 5 times and applied iterative region-growing to the remaining WM voxels until they met a GM voxel; **G)** A nonlinear registration and label-fusion approach [9] was used to mask out uninteresting structures: deep GM, ventricles and the periventricular germinal zone (which looks like GM as neural cells extend into this area in neonates) and the cerebellum. While the cerebellum was removed, other masked structures were merged into the WM class; **H)** Segmentation of the corpus callosum in the mid-plane divided

the WM into hemispheres. This separation allowed for analysis of hemispheric asymmetry in morphometry by co-registering the flipped right hemisphere to the left; **I**) we parameterized the WM boundary by evolving an ellipsoid, triangulated using an icosahedral model and a multi-resolution deformation scheme, as in the CIVET [3]; **J**) To improve point correspondence across subjects, a surface-based registration [5] was performed with respect to age-specific templates; **K**) The cortical morphology was characterized by measuring mean curvature; **L**) Finally, these measurements were further re-sampled to the surface template using the transformation obtained in the surface registration, in order to allow inter-subject comparison.

In the following sections, we describe the new modules included in NEOCIVET and how they address technical challenges in neonatal brain MRI. We also discuss the choice of parameters for optimal performance. Finally, using a large dataset of preterm-born neonates we investigate the ability of NEOCIVET to assess developmental trajectory and its clinical utility.

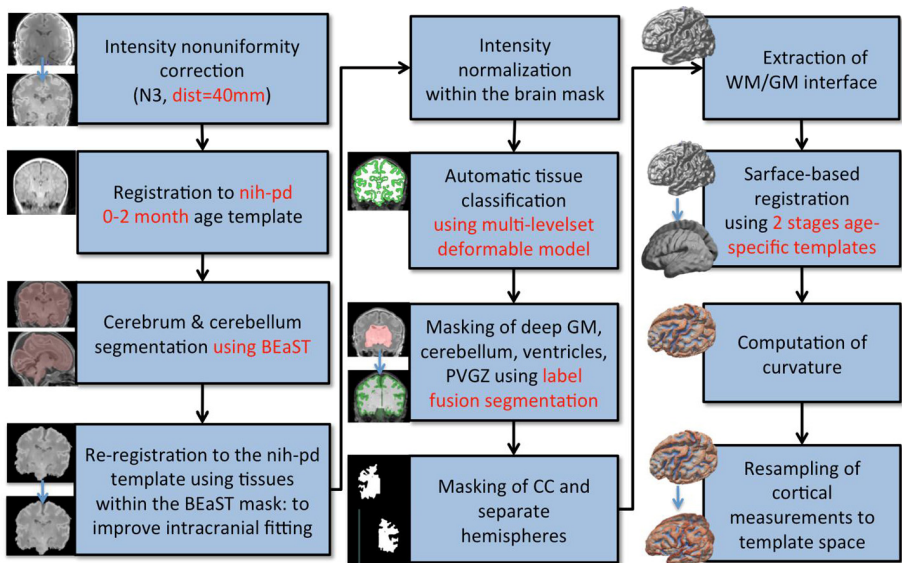


Fig. 1. Flowchart of NEOCIVET, a variant of CIVET used for neonatal brain analysis. New modules and parameters are in red. PVGZ: periventricular germinal zone.

2.1 Subjects and MRI Acquisition

Our initial dataset comprised 52 preterm newborns (mean postmenstrual age [PMA]= 28.7 ± 1.8 wks; range 24.7-32.2 wks), admitted to UCSF Benioff Children's Hospital San Francisco between July 2011 and June 2014. All patients were scanned post-natally as soon as clinically stable, and 30 patients were re-scanned before discharge at late preterm age (34-38 wks corrected gestational age). Due to severe motion artifact, 9 baseline and 8 follow-up scans were excluded. The final database included 43 baseline (PMA= 32.3 ± 2.0 wks) and 22 follow-up scans (35.9 ± 1.5 wks). 3T MRI scans were acquired using a specialized high-sensitivity neonatal head coil

built within an MRI-compatible incubator. T1-weighted images were acquired using sagittal 3-dimensional inversion recovery spoiled gradient echo (TR = minimum; TE = minimum; FOV = 180°; NEX = 1.00; FA = 15°), yielding images with 0.7x0.7x1mm³ spatial resolution.

2.2 Classification of Brain Tissues

We expanded Li’s deformable model [6] to constrain it for cortical GM segmentation. Let a given image be $I: \Omega_i \rightarrow \mathfrak{R}$. Ω_i ($i=1, 2$) is a region that defines foreground ($i=1$) or background ($i=2$). For a given 3D point $\mathbf{x} \in \Omega$ and intensity $I(\mathbf{x})$, Li’s level-set formula is defined as:

$$\frac{\partial \phi}{\partial t} = -\delta_\epsilon(\phi)(\lambda_1 e_1 - \lambda_2 e_2) + v\delta_\epsilon(\phi)\nabla \cdot \left(\frac{\nabla \phi}{|\nabla \phi|}\right) + \mu \left(\nabla^2 \phi - \nabla \cdot \frac{\nabla \phi}{|\nabla \phi|}\right) \tag{1}$$

where δ_ϵ is the smoothed Dirac delta function and e_1 and e_2 are terms combining global and local intensity fitting energy and are expanded as:

$$e_i(\mathbf{x}) = \int_{\Omega_i} K_\sigma(\mathbf{y} - \mathbf{x}) |I(\mathbf{y}) - f_i(\mathbf{x})|^2 d\mathbf{y}, \quad i = 1, 2 \tag{2}$$

K is 3D Gaussian kernel function that is centered at \mathbf{x} and is scalable using σ ($\sigma > 0$). $f_1(\mathbf{x})$ and $f_2(\mathbf{x})$ are two values that approximate image intensities within Ω_1 and Ω_2 . The term $\delta_\epsilon(\phi)(\lambda_1 e_1 - \lambda_2 e_2)$ in Eq (1) evolves the level-set to the regional boundary whereas the other terms maintain the regularity of the level-set. More details are found in the original publication [6].

To optimize GM/WM segmentation, we feed the algorithm an initial segmentation based on the EM algorithm performed on the whole brain (Fig. 2B). We also enhance the image $I(\mathbf{x})$ using non-local de-noising: $I'(\mathbf{x}) = NL(I(\mathbf{x}))$. Some cortical areas consistently appeared to be dark or thin in the MRI due to chemical shift misregistration. To address this, we introduced a cortical thickness constraint. The cortical thickness $T(\mathbf{x})$ is computed by the Laplacian transform within the GM mantle as in [10]. We invert this as:

$$T^{-1}(\mathbf{x}) = \frac{1}{T(\mathbf{x})} \text{ if } T(\mathbf{x}) > 0; \quad T^{-1}(\mathbf{x}) = 0 \text{ if } T(\mathbf{x}) = 0 \tag{3}$$

A large T^{-1} describes voxel clusters of the “artificially” thin or missing cortex. Finally $I(\mathbf{x})$ in Eq. (2) is replaced with $I'(\mathbf{x}) + \lambda_{thick} \tilde{T}^{-1}(\mathbf{x})$, where $\tilde{T}^{-1}(\mathbf{x}) = K_{\sigma T}(T^{-1}(\mathbf{x}))$ is a smooth version of T^{-1} (Fig. 2C) and λ_{thick} is a weight constant. The thickness was re-computed every 40 iterations. An improved segmentation is illustrated in Fig. 2E.

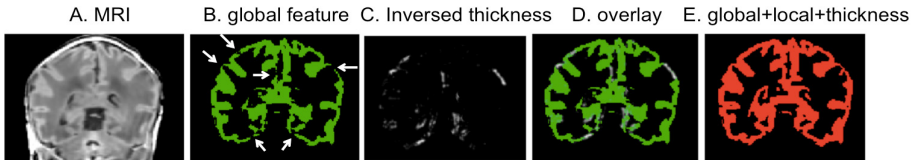


Fig. 2. Tissue classification. Initial segmentation using a global histogram shows missing GM voxels (arrows). Combining the inverted thickness constraint with local contrast term in the level-set formulation makes a marked recovery in GM segmentation and topology (red).

2.3 Surface Fitting

The WM/GM interface was extracted by deforming an ellipsoid triangulated using icosahedral sampling [4]. The initial surface was sampled with 320 triangles and deformed towards the boundary of the hemispheric WM. The surface was up-sampled to 81,920 triangles at the end of each deformation cycle.

2.4 Surface-Based Morphological Measurements

In most applications, CIVET is primarily used to measure cortical thickness between the inner and outer cortical surfaces. In contrast, NEOCIVET aims to characterize the cortical folding at the WM/GM interface (=inner surface) by computing mean curvature that captures concavity/convexity (Fig. 3).

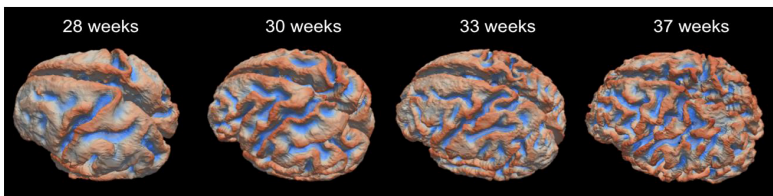


Fig. 3. Mean curvature as cortical folding measurement.

2.5 Construction of Age-Specific Surface Templates and Registration

As seen in Fig. 3, cortical folding changes dramatically during perinatal development. This emphasizes the importance of constructing templates that capture the precise cortical morphology at specific age ranges, so as to ensure the accuracy of registration. We therefore subdivided our dataset into four age ranges: 28-30 (n=12), 31-33 (n=15), 34-36 (n=19) and 37-40 (n=13) weeks PMA. For each group, we constructed a surface template using *SURFTRACC*, a surface registration algorithm included in CIVET [5] and an unbiased template construction framework [11]. In brief, *SURFTRACC* first transposes individual sulcal depth maps into icosahedral spheres. It then iteratively searches for local optimal vertex correspondence between an individual and a template sphere based on a matching of a given feature (in this case, depth potential function [12]). Mapping the deformed meshes back to the original cortical surface coordinates allows a registration of the individual to the template surface. Inclusion of a regularization step further preserves local surface topology. This procedure was integrated into a hierarchical framework that allows for registration from coarse to fine scale. An initial template was created by a simple averaging of vertices among the surfaces in each age group. Thereafter, an iterative alignment proceeds from low dimensional warping of all individuals to the initial template, and towards higher dimensional warping to a new template that is constructed from the previous warping cycle (similar to the process shown in Table). Left and “flipped-right” hemispheres from all subjects were pooled to avoid subject- and hemisphere-specific bias in the

evolution and averaging. After construction, the youngest-age template was registered to the 2nd youngest and so on such that each template was registered to its closest older template, yielding a temporally continuous transformation. For inter-subject analyses, any given subject was first registered to the corresponding age template and then was ultimately transformed to the oldest template space (shown in Fig. 4-5) by concatenating the sequence of transformations between age-specific templates.

2.6 Other Technical Considerations and Parameter Selection

For optimal performance in our neonatal dataset, parameters in the NEOCIVET were empirically chosen. Also, some CIVET modules were updated with more recent publicly available techniques. Below, we describe these modifications in some detail so as to guide NEOCIVET users in their parameter selection with respect to MRI field strength, pulse sequence and spatial resolution:

a) For intensity inhomogeneity correction using N3, we found that a smoothing distance for RF wavelength as 40mm yielded best performance in brain masking and tissue classification, which also agreed with the result from a previous extensive analysis using 3T MRI data [13].

b) The FSL-BET-based brain masking and single atlas-based masking of deep GM and ventricles performed poorly for neonatal brains due to rapid changes in volume and intensity. We addressed this issue by introducing publicly available techniques that use patches of multiple templates or fuse multiple templates based on a similarity measure [8, 9]. The use of a minimum of 15-20 manually labeled atlases for various age ranges achieved excellent segmentation accuracy (Dice>0.87%).

c) Our data were scanned with an in-plane resolution of $0.7 \times 0.7 \text{mm}^2$ with 1mm thickness whereas the NIH neonatal template was sampled at 1mm^3 . Registration to this template caused image data loss. We thus up-sampled this template to $0.5 \times 0.5 \times 0.5 \text{mm}^3$. However, this step did not necessarily improve registration, which was optimized ultimately using the age-specific surface templates described in 2.5.

d) Parameters in the level-set tissue segmentation were chosen empirically as: $\lambda_1=1$, $\lambda_2=1$, $\lambda_{\text{thick}}=1$, $\sigma=3$, $\sigma_f=1$, $\epsilon=1$, $\mu=1$, $\nu=12.5$, time step=0.005, #iteration=400. On a single core of IntelTM i7-3770K, 3.5GHz, the segmentation step and the whole pipeline process for a neonatal MRI took 10 minutes and 2.1 hours, respectively.

3 Application and Clinical Utility of NEOCIVET

Here, we investigated the ability of the pipeline to assess developmental trajectory and the impact of brain injury on cortical structural development.

3.1 Statistical Analyses

Statistical analysis was performed using SurfStat (<http://www.math.mcgill.ca/keith/surfstat/>). Mixed-effect linear models were used to address both inter-subject effects and within-subject changes between serial MRI scans by permitting multiple measurements per subject and thus increasing statistical power. We assessed

developmental trajectory of cortical complexity by correlating the magnitudes of sulcal depth and curvature with postmenstrual age (PMA) at the time of scanning. Given that severe perinatal WM injury (WMI) often disrupts postnatal brain growth, we assessed the association between cortical complexity changes and the presence of WMI (a score of 2 or higher on the clinical grading system). To this end, we used a linear model that included WMI and PMA as independent variables and cortical measurements as the dependent variable set. We then analyzed an interaction term of WMI x PMA. Multiple comparisons were adjusted using false discovery rate [14].

3.2 Results

NEOCIVET identified significant increases in cortical folding in numerous cortical regions in relation to growth in preterm-born neonates (mean curvature: + 0.004/wk), whilst folding did not change in major sulci (Sylvian, central, parieto-occipital, and calcarine fissures) that are known to develop early (corrected $p < 0.05$; Fig. 4) [15].

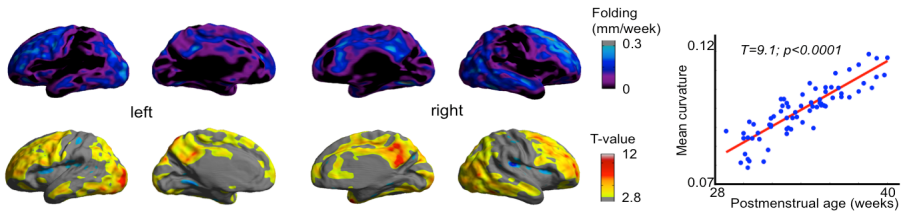


Fig. 4. Developmental trajectory of cortical folding. Left: Patterns show increased sulcal folding/week (top) and the significance map in T-value ($p < 0.05$; bottom); Right: Plotted is mean curvature changes versus increase in PMA in the areas displaying significance.

In broad areas, including both early and late developing cortices, the cortical folding increase was disrupted in the presence of severe perinatal WMI ($p < 0.001$; Fig. 5). The pattern of folding disruption was hemispherically symmetric. WMI is known to occur perinatally, mostly in the late second and the third trimester. The broad effect of WMI even on some of major sulcal areas may indicate disruption of late neuronal or astrocyte migration.

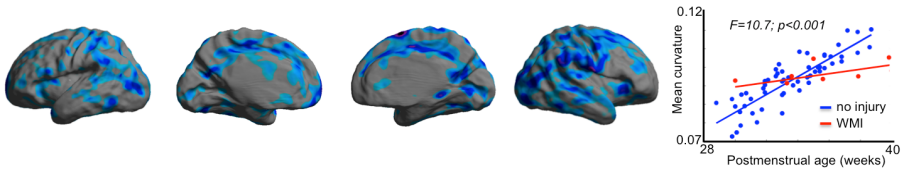


Fig. 5. Disrupted postnatal cortical folding in relation to severe WMI. Significant disruption is found in areas in blue ($T > 2.8$; corrected $p < 0.05$).

4 Discussion and Conclusion

We have proposed NEOCIVET, a variant of the CIVET pipeline that was designed to extract the cortical surface and measure relative morphometrics, for application to neonatal MRI. NEOCIVET successfully characterized the developmental trajectory of cortical folding by improving a series of processes in CIVET. NEOCIVET revealed cortical developmental disruption in the presence of perinatal WMI, demonstrating its potential to provide biomarkers of prematurity-related developmental outcome.

Volumetric registration can be biased by differences in anatomical maturation between preterm babies and the normal neonatal template. However, the volume registration in our analysis was only for coarse spatial normalization, specifically for brain size. The size normalization combined with use of a fixed number of vertices in surface modeling should minimize bias related to maturation that affects the parameters in segmentation and depth potential calculation for surface registration. Maturation-related anatomical variability was further addressed in the surface space where we measure actual cortical folding, using age-specific preterm brain templates.

The main weakness of the contemporary fetal/neonatal pipelines is using age-specific tissue probability maps to correct for local tissue intensity variations [16], which can bias the tissue segmentation in abnormal brains. Another weakness is the lack of point-wise correspondence between subjects, which challenges group-wise analysis of regional changes [1-2]. We overcame these weaknesses using a segmentation method with a local tissue contrast model without prior information as well as a surface registration technique that re-arranges mesh triangulation based on cortical folding similarity between subjects, thus optimizing point correspondence.

We note that the current set of templates is preliminary, as Lyttelton et al. [11] pointed out that a minimum of 30 subjects is required for a stable template construction. We are currently recruiting more preterm-born neonates and plan to re-create those templates with a sufficient sample size. We plan to include NEOCIVET in a future CIVET release that is open to the public through CBRAIN, a web-based platform for distributed processing and exchange of 3D/4D brain imaging data (<http://mcin-cnim.ca/neuroimagingtechnologies/cbrain/>).

References

1. Wright, R., Kyriakopoulou, V., Ledig, C., Rutherford, M.A., et al.: Automatic quantification of normal cortical folding patterns from fetal brain MRI. *Neuroimage* 91, 21–32 (2014)
2. Melbourne, A., Kendall, G.S., Cardoso, M.J., Gunny, R., et al.: Preterm birth affects the developmental synergy between cortical folding and cortical connectivity observed on multimodal MRI. *Neuroimage* 89, 23–34 (2014)
3. Kim, J.S., Singh, V., Lee, J.K., Lerch, J., et al.: Automated 3-D extraction and evaluation of the inner and outer cortical surfaces using a Laplacian map and partial volume effect classification. *Neuroimage* 27(1), 210–221 (2005)
4. MacDonald, D., Kabani, N., Avis, D., Evans, A.C.: Automated 3-D extraction of inner and outer surfaces of cerebral cortex from MRI. *Neuroimage* 12(3), 340–356 (2000)

5. Robbins, S., Evans, A.C., Collins, D.L., Whitesides, S.: Tuning and comparing spatial normalization methods. *Med. Image Anal.* 8(3), 311–323 (2004)
6. Li, C.M., Kao, C.Y., Gore, J.C., Ding, Z.H.: Minimization of region-scalable fitting energy for image segmentation. *IEEE Transactions on Image Processing* 17(10), 1940–1949 (2008)
7. Sled, J.G., Zijdenbos, A.P., Evans, A.C.: A nonparametric method for automatic correction of intensity nonuniformity in MRI data. *IEEE Trans. Med. Imaging* 17, 87–97 (1998)
8. Eskildsen, S.F., Coupe, P., Fonov, V., Manjon, J.V., et al.: BEaST: brain extraction based on nonlocal segmentation technique. *Neuroimage* 59(3), 2362–2373 (2012)
9. Wang, H.Z., Suh, J.W., Das, S.R., Pluta, J.B., et al.: Multi-Atlas Segmentation with Joint Label Fusion. *IEEE Trans. on Pattern Analysis and Machine Intelligence* 35(3), 611–623 (2013)
10. Jones, S.E., Buchbinder, B.R., Aharon, I.: Three-dimensional mapping of cortical thickness using Laplace’s equation. *Hum. Brain Mapp.* 11(1), 12–32 (2000)
11. Lyttelton, O., Boucher, M., Robbins, S., Evans, A.: An unbiased iterative group registration template for cortical surface analysis. *Neuroimage* 34(4), 1535–1544 (2007)
12. Boucher, M., Whitesides, S., Evans, A.: Depth potential function for folding pattern representation, registration and analysis. *Medical Image Analysis* 13(2), 203–214 (2009)
13. Boyes, R.G., Gunter, J.L., Frost, C., Janke, A.L., et al.: Intensity non-uniformity correction using N3 on 3-T scanners with multichannel phased array coils. *Neuroimage* 39(4), 1752–1762 (2008)
14. Benjamini, Y., Hochberg, Y.: Controlling the false discovery rate: a practical and powerful approach to multiple testing. *J. Royal Stat. Soc.* 57(1), 289–300 (1995)
15. Kostovic, I., Vasung, L.: Insights from in vitro fetal magnetic resonance imaging of cerebral development. *Semin. Perinatol.* 33(4), 220–233 (2009)
16. Habas, P.A., Scott, J.A., Roosta, A., Rajagopalan, V., et al.: Early folding patterns and asymmetries of the normal human brain detected from in utero MRI. *Cereb. Cortex* 22(1), 13–25 (2012)